JACS
JOURNAL OF THE AMERICAN CHEMICAL SOCIETY

Article

pubs.acs.org/JACS

Transition Metal Dichalcogenide Atomic Layers for Lithium Polysulfides Electrocatalysis

Ganguli Babu, Nirul Masurkar, Hesham Al Salem, and Leela Mohana Reddy Arava*

Department of Mechanical Engineering, Wayne State University, Detroit, Michigan 48202, United States

Supporting Information

ABSTRACT: Lithium−sulfur (Li−S) chemistry is projected to be one of the most promising for next-generation battery technology, and controlling the inherent "polysulfide shuttle" process has become a key research topic in the field. Regulating intermediary polysulfide dissolution by understanding the metamorphosis is essential for realizing stable and high-energy-density Li−S batteries. As of yet, a clear consensus on the basic surface/interfacial properties of the sulfur electrode has not been achieved, although the catalytic phenomenon has been shown to result in enhanced cell stability. Herein, we present evidence that the polysulfide shuttle in a Li−S battery can be stabilized by using electrocatalytic transition metal dichalcogenides (TMDs). *Physicochemical* transformations at the electrode/electrolyte interface of atomically thin monolayer/few-layer TMDs were elucidated using a combination of spectroscopic and microscopic analysis techniques. Preferential adsorption of higher order liquid polysulfides and subsequent conversion to lower order solid species in the form of dendrite-like structures on the edge sites of TMDs have been demonstrated. Further, detailed electrochemical properties such as activation energy, exchange current density, rate capabilities, cycle life, etc. have been investigated by synthesizing catalytically active nanostructured TMDs in bulk quantity using a liquid-based shear-exfoliation method. Unveiling a specific capacity of 590 mAh g^{-1} at 0.5 C rate and stability over 350 cycles clearly indicates yet another promising application of two-dimensional TMDs.

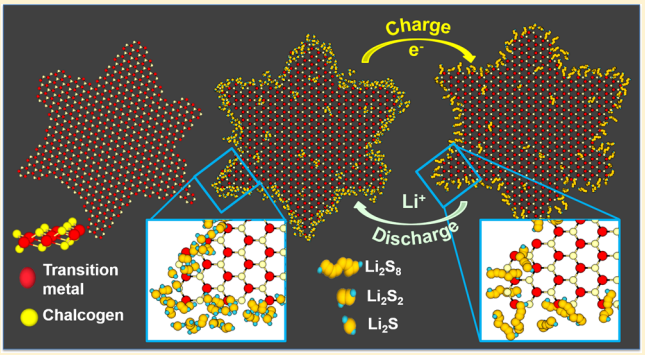

1. INTRODUCTION

Energy storage, being a critical component of many innovative technologies, has been a highly studied field and calls for rapid improvements. Advances in battery technology have been the driving force behind concepts such as electric vehicles and renewable energy for the grid. The search for better battery technologies has involved exploration of various mechanisms and chemistries superior to the existing types.[1−5] Of the various alternatives, lithium−sulfur (Li−S) chemistries are among the most promising for the next-generation battery technology, owing to advantages such as high theoretical capacity of 1672 mAh g^{-1} (10 times higher than that of conventional Li-ion battery cathodes), non-toxicity, and low cost of sulfur.[6−11] However, the insulating nature of sulfur, dissolution of intermediate polysulfides into the electrolyte, and sluggish kinetics during their conversion reactions pose serious challenges in attaining the cycle life and rate capability required for commercial applications.[1]

The past decade has witnessed intense research efforts to stabilize the polysulfide shuttle process mainly by physically constraining the sulfur within the pores of various carbon materials, but the low active material loading in these electrodes and their poor adsorption toward polysulfides have resulted in limited success.[12−14] These unsolved issues warrant a critical need for a fundamental breakthrough to stabilize the polysulfide shuttle process. Recently, we have proposed an electrocatalytic approach to Li−S batteries, showing the activity of metals like Ni, Au, and Pt to enhance reaction kinetics and also stabilize the polysulfide shuttle process.[15,16] Further, we have found that the presence of an electrocatalyst in a composite electrode (Pt/graphene) exhibited reduced overpotential and an improved specific retention capacity over pristine electrodes. Although this innovative take on cell design has improved the electrochemical performance, the high cost of Pt electrocatalyst and the limitation on available catalytically active sites posed restrictions on the sulfur loading (catholyte concentration) in the cell.

In searching for an efficient and cost-effective electrocatalyst as an alternative to noble metals, two-dimensional transition metal dichalcogenide (TMD; for example, XS_2, with X = Mo, W) materials were found to be attractive due to their long record as a catalyst in hydro-desulfurization,[17] solar cells,[18,19] photocatalysis, and hydrogen evolution reactions[18,20−23] and their stability toward sulfur chemistries.[24−26] XS_2 materials specifically showed synergism among metal d-orbitals, and the unsaturated heteroatom (such as sulfur) results in an effective d-band structure, imparting catalytic characteristics approaching the d-band of Pt. The catalytic activity of these materials for a

Received: August 19, 2016
Published: December 6, 2016

DOI: 10.1021/jacs.6b08681
J. Am. Chem. Soc. 2017, 139, 171−178

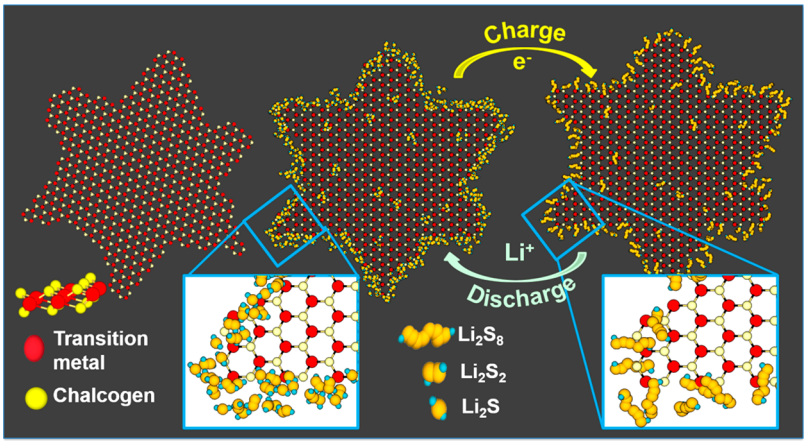

Figure 1. Schematic illustration of chemical vapor deposition-grown transition metal dichalcogenide nanosheets for Li−S battery, showing confined deposition of lithium polysulfides at preferential catalytic sites and their conversions during discharge−charge processing in a catholyte solution.

reaction was correlated to the number of exposed edge sites that have unique chemical and electronic structure compared to their respective basal planes (0001).[27] Hence, it is a prerequisite to design and improve the preferential catalytic active sites (edge sites) for efficient reaction kinetics. Considerable efforts were made to maximize the aspect ratio of active catalytic sites in XS_2 materials through the design and synthesis process, including the use of nanoparticles, porous structures, nanowires, and hybrid heterostructures.[21,28−32] Among the various configurations, atomically thin layered structures have emerged recently as an exciting area of catalytic activity due to the high aspect ratio of edge sites and accessibility of a large catalytic surface.

To the best of our knowledge, there are no reports on utilizing XS_2 (X = W, Mo) nanosheets as electrocatalysts for lithium polysulfide (LiPS) conversion reactions. Herein, we illustrate our efforts to understand the interactions between the electrocatalyst and polysulfide species using chemical vapor deposition (CVD)-grown WS_2 and MoS_2 flakes, as they contain higher ratios of catalytically active edge sites (Figure 1). Further, a shear-exfoliation method was used to produce WS_2 nanosheets on a large scale to imitate the electrocatalysis-driven performance in order to meet the commercial demand of the battery industry. The adsorption of LiPS onto the electrode surface and the electrocatalytic and electrochemical properties of WS_2 nanosheets were studied in detail. We believe that electrocatalysis of polysulfides using inexpensive materials such as WS_2 and MoS_2 nanosheets will open a new avenue for developing efficient energy storage technologies.

2. EXPERIMENTAL METHODS

2.1. Chemical Vapor Deposition Growth of Few-Layer XS_2 (X = W, Mo) Flakes. WS_2/MoS_2 monolayer and few-layer flakes were grown on clean 300 nm SiO_2/Si substrate by using CVD. Initially, substrate was cleaned in acetone, isopropyl alcohol, and de-ionized water. The samples were then loaded in a 2-in. CVD furnace and placed face down above a porcelain crucible containing sprinkled WO_3/MoO_3 powder (Sigma-Aldrich). Another crucible containing sulfur was placed upstream at the end of the furnace. WS_2 CVD growth was conducted at atmospheric pressure while flowing 16% H_2 in argon at 850 °C, whereas MoS_2 nanosheets were grown with pure argon at 750 °C.[33,34] To make an electrical connection to the as-grown nanoflakes, we transferred them to pre-patterned aluminum tracks (50 nm thickness) on SiO_2/Si using UV lithography. The suspended flakes in KOH solution were then transferred carefully to patterned aluminum tracks without losing the alignment, as shown in scanning electron microscopy (SEM) images. Prior to assembly of the electrochemical cell, wire-bonding was performed to obtain electrical contacts to the transferred nanoflakes on the aluminum tracks.

2.2. Shear Exfoliation of WS_2. In a typical experiment, bulk WS_2 (2 μm, Sigma-Aldrich) was dispersed in an aqueous solution of sodium cholate (surfactant, Sigma-Aldrich). The optimized ratio between bulk WS_2 and surfactant is 5:1 (25:5 g) in 500 mL of Millipore water for each shear-exfoliation process in a high-shear-rate blender (Vitamix). To avoid re-stacking of exfoliated WS_2 nanosheets due to overheating of the solution, the mixing was performed for 2 min with an interval rest-time of 2 min in an ice-cold bath. The same cycling process was continued for 6 h to obtain WS_2 nanosheets in surfactant solution. First, well-dispersed 2D nanosheets were separated from un-exfoliated WS_2 by centrifugation at as low as 1500 rpm. The concentrated supernatant liquid containing few-layer WS_2 was purified and further concentrated by centrifuging at 12 000 rpm for 30 min. Finally, 2D nanosheets were collected after filtration using 0.02 μm pore size membrane, rinsed with copious amounts of water to remove surfactant from the exfoliated nanosheets, and dried under a vacuum for 12 h prior to investigating their physicochemical and electrochemical properties.

2.3. Preparation of Lithium Polysulfides (Li_2S_4 and Li_2S_8). For LiPS adsorption and electrocatalytic studies, 10 mM Li_2S_4 solution was made by reacting stoichiometric amounts of Li_2S and S in 1:1 v/v of 1,3-dioxalane and 1,2-dimethoxyethane at 50 °C for overnight. The electro-active species containing catholyte solution (600 mM) for electrochemical properties was prepared using calculated amounts of Li_2S and S to attain a nominal formula of long-chain LiPS (Li_2S_8) in tetraethylene glycol dimethyl ether (TEGDME) at 90 °C for 12 h or until all the solid particles dissolved. These molar concentrations are calculated on the basis of the amount of active species, i.e., sulfur, in LiPS solution.

2.4. Adsorption and Electrocatalytic Studies. Two Li_2S_4−WS_2 solutions were prepared along with a blank solution (only LiPS as controlled experiment) to examine the polysulfides' adsorption on WS_2 nanosheets. In a typical process, 250 and 500 μg portions of WS_2 were dispersed individually in 1:1 v/v of 1,3-dioxalane and 1,2-dimethoxyethane, and the same was added to 1 mL of LiPS (Li_2S_4) solution with stirring for 30 min. To observe color changes in solution, the mixtures were left undisturbed for 12 h. The supernatant and WS_2 nanosheets (precipitate) were studied by ultraviolet−visible (UV−vis) spectrophotometry and X-ray photoelectron spectroscopy (XPS), respectively. The electrocatalytic activity of WS_2 toward LiPS conversion reactions was measured using voltammetry techniques (cyclic voltammetry (CV), potentiostatic, and linear sweep voltammetry (LSV)) on a three-electrode cell, consisting of WS_2-coated glassy carbon (GC) as the working electrode, lithium foil as counter/reference electrode, and 10 mM Li_2S_4 solution as an electrolyte. An electrocatalyst

DOI: 10.1021/jacs.6b08681
J. Am. Chem. Soc. 2017, 139, 171−178

was loaded on GC using 5 wt% Nafion solution as reported previously in the literature.

2.5. Cell Fabrication and Electrochemical Measurements. Electrocatalytically active electrodes were prepared by appropriately mixing bulk WS_2 or shear-exfoliated WS_2 individually with conductive carbon (Super-P) and polyvinylidene fluoride (PVDF) binder in a weight ratio of 80:10:10. That composite was made into a slurry using *N*-methyl-2-pyrrolidone (NMP) as solvent and coated uniformly on 18 μm thin aluminum foil. The electrode-coated Al foil was dried in a vacuum oven at 90 °C to evaporate NMP and cut into circular discs of 12.7 mm diameter. Standard 2032 coin cells were fabricated to measure electrochemical properties using coated WS_2 materials as working electrode, lithium metal as counter/reference electrode, and celgard separator. A pre-calculated amount of 600 mM catholyte containing 1.56 mg of sulfur was used as the active material, along with an electrolyte consisting of 1 M lithium bis(trifluoromethanesulfonyl)-imide (LiTFSI) and 0.5 M lithium nitrate ($LiNO_3$) in TEGDME. LSV and CV studies were conducted using a VMP3 potentiostat (Biologic Science Instruments) in the potential window of 3.0−1.5 V at a scan rate of 0.1 mV s^{-1}. Galvanostatic charge−discharge studies were performed for WS_2 electrodes at different current rates in the potential range of 1.5−3.0 V using an ARBIN charge−discharge cycle life tester.

2.6. Characterizations. X-ray diffraction (XRD) patterns were recorded at a scan rate of 0.03° s^{-1} on a Rigaku Miniflex II X-ray diffractometer using a Cu Kα source. Surface morphology (field emission electron microscopy images) studies were performed on a JEOL JSM-7600 system operated with an accelerating voltage of 20 kV. X-ray photoelectron spectra of electrode surfaces were collected using a PHI Quantera spectrophotometer. Transmission electron microscopy (TEM) images were recorded on a JEOL 2010 transmission electron microscope using a LaB_6 filament gun. Raman studies were carried out on Triax 550 (Horiba JobinYvon, Edison, NJ) with 514 nm laser excitation.

3. RESULTS AND DISCUSSION

3.1. Exploration of Catalytic Active Sites on XS_2 (X = W, Mo) Nanosheets. To illustrate preferential sites for LiPS adsorption and their conversions, few-layer WS_2 and MoS_2 nanosheets were grown using tungsten oxide/molybdenum oxide with evaporated sulfur on SiO_2/Si substrate at 850 °C/750 °C, respectively. Such full-fledged nanosheets were characterized by optical microscopy and Raman spectroscopy, and the obtained results are shown in the Supporting Information (Figures S1 and S2). Optical images reveal the formation of triangle-and star-like structured WS_2 films with large area continuity and uniformity, analogous to the films that were previously reported.[35,36] The prominent Raman-active modes were identified at 356.2 and 426.3 cm^{-1} for WS_2 and 388.6 and 411.4 for MoS_2, corresponding to in-plane (E_{2g}^1) and out-of plane (A_g^1) vibrations of W/Mo and S atoms (Supporting Information, Figure S2). Further, the difference in frequencies of the two characteristic Raman modes for WS_2 (70.1 cm^{-1}) and MoS_2 (22.8 cm^{-1}) confirms that the synthesized nanosheets were composed of two to three layers.[37−39]

To investigate preferential active sites of XS_2 (X = W, Mo) nanosheets for LiPS adsorption and their catalytic conversion reactions, CVD-synthesized flakes were transferred to pre-patterned aluminum tracks on SiO_2/Si substrate (Supporting Information, Figure S3). Prior to immersing WS_2 nanosheet-containing substrate into LiPS catholyte solution for electrochemical reactions, wire bonding was carried out to ensure electrical connections. A typical three-electrode electrochemical cell was assembled using such WS_2 and MoS_2 nanosheets as working electrodes individually against metallic lithium as counter/reference electrode in catholyte solution (TEGDME) containing 10 mM Li_2S_4, 1 M LiTFSI, and 0.1 M $LiNO_3$. The galvanostatic discharge process was performed at a current rate of 10 μA to understand the LiPS adsorption and catalytic active sites on nanosheets. As expected, we observed controlled adsorption of discharge products predominantly at edge sites of XS_2 (X = W, Mo) nanosheets (Figure 2). Such spatially localized adsorption initiates due to the presence of unsaturated sulfur atoms at the edge sites, promoting electron transfer to occur for polysulfides' conversion reactions. As a result, short-chain LiPS was deposited systematically at the end of the discharge process with dendrite-like structure, as evidenced from the SEM image (Figure 2a). It is clearly seen from the magnified image in Figure 2a that the WS_2 nanosheet (before discharge) has an unbroken edge plane about tens of μm in length, in contact with conductive tracks. Upon discharge, edge sites all over the flake were completely covered by LiPS

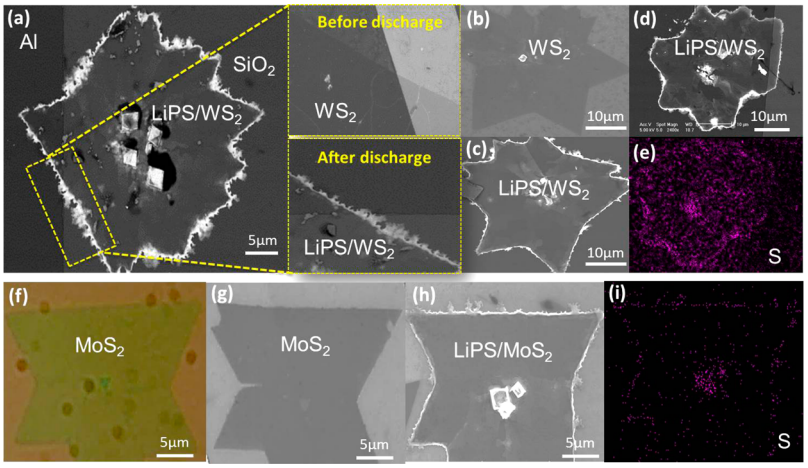

Figure 2. Exploration of preferential catalytic sites of XS_2 (X = W, Mo) nanosheets for LiPS conversion reactions. (a) SEM image of short-chain LiPS deposition at catalytic edge sites of WS_2 nanosheets in communication with a conductive aluminum track on SiO_2/Si substrate during the discharge process. (b,c) Comparative images of pristine WS_2 nanosheets (before discharge) and controlled adsorption of LiPS on nanosheets (after discharge). (d,e) Sulfur elemental mapping and corresponding SEM image of WS_2 nanosheets in the discharged state. (f,g) Optical and SEM images of MoS_2 flakes as-grown by the CVD process. (h) Directional deposition of LiPS on MoS_2 flakes from (g) at the discharged state. (i) Elemental of mapping of sulfur on MoS_2−LiPS flake (h).

DOI: 10.1021/jacs.6b08681
J. Am. Chem. Soc. 2017, 139, 171−178

deposition, confirming the preferential sites for polysulfides' conversion reactions.

Similarly, the controlled deposition of LiPS with dendrite-like morphology at the edge sites of another nanosheet is compared in Figure 2b,c. Unlike random deposition of short-chain polysulfides in sulfiphobic electrode-based cells, here organized deposition of polysulfides along the axis of the edge planes retains electrical contact with the cathode matrix, which suppresses the active material loss and improves LiPS reversibility.[13] In the EDAX mapping, the concentration of sulfur distribution was found to be more prominent on the edge planes, as observed in the corresponding SEM image, which confirmed their higher catalytic activity compared to the counterpart basal planes (Figure 2d,e). In addition, the versatility of the present approach was verified using similar experiments on CVD-grown MoS_2 nanosheets, wherein short-chain LiPS deposited typically in a dendrite-like arrangement at edge sites (Figure 2f–i). Hence, a higher number of exposed catalytic sites at the edge plane is desirable to improve the Li–S battery performance; this is in good agreement with reports on similar materials for hydrogen evolution reactions[40,41] and Li_2S electrodeposition.[42]

Though the CVD process is desirable to grow high-quality nanosheets with definite morphology and layer orientation, its ability to be scaled up for energy storage applications is still arguable. In this context, a liquid exfoliation method was considered as one of the most effective ways to achieve large-scale production of nanosheets of layered materials.[43,44] Herein, further studies are focused on tungsten disulfide which was exfoliated by shear exfoliation (large scale) in aqueous surfactant solution using a high shear rate blender.[45,46] The resulting WS_2 nanosheets were used for various studies, such as adsorption of dissolved LiPS, electrocatalytic activity, and electrochemical reversibility during LiPS conversion reactions.

3.2. Shear-Exfoliated WS_2 Nanosheets for LiPS Conversion Reactions. The shear-exfoliated WS_2 nanosheets, along with their bulk counterpart, were systematically characterized using SEM, XRD, and XPS studies. For the shear process, a significant reduction in thickness and flake size of WS_2 represents a successful exfoliation in aqueous surfactant solution. Such exfoliated flakes were observed along with extensive wrinkling at the edges due to the forces generated by the high shear rate (Supporting Information, Figure S4). Details pertinent to XRD and XPS characterization of shear-exfoliated nanosheets are given in the Supporting Information (Figures S5 and S6). Unlike other liquid exfoliation methods, shear exfoliation resulted in a small lateral size, well below 100 nm, which is widely accepted for efficient electrocatalysis.[47] Similarly, TEM images (Figure 3a,b) showed a narrow distribution in the lateral dimensions of the nanosheets.

In order to elucidate the electrocatalytic properties of WS_2 toward polysulfides, fundamental electrochemical studies such as CV, LSV, and potentiostatic polarization were performed using Li_2S_4 as the representative polysulfide species in a three-electrode assembly. Critical catalytic parameters such as redox currents, onset potentials, and exchange current densities were obtained from the WS_2 electrode, and the results were compared with those from the carbon electrode. Figure 3c,d displays the representative CV performance and Tafel plots of WS_2 nanosheets and carbon electrode. The derived parameters, i.e., onset potentials (E_{pa}, E_{pc}) and peak current densities (I_{pa}/I_{pc}), along with exchange current density values are given in Table 1. For WS_2 nanosheets, the observed onset potentials related to reduction of LiPS were 2.24 and 1.78 V, which was a positive shift compared to those of the carbon electrode (2.21 and 1.67 V) in identical experimental conditions. Similarly, the observed onset potential corresponding to oxidation of LiPS with WS_2 electrode was 2.39 V, a negative shift compared to 2.42 V for the carbon electrode. Such a high cathodic potential and low anodic potential were indications of low polarization and improved lifetime of the battery.

In addition, LiPS redox peak current densities of WS_2 electrode were much higher than those of the carbon electrode, demonstrating the high catalytic activity of the WS_2 electrode.

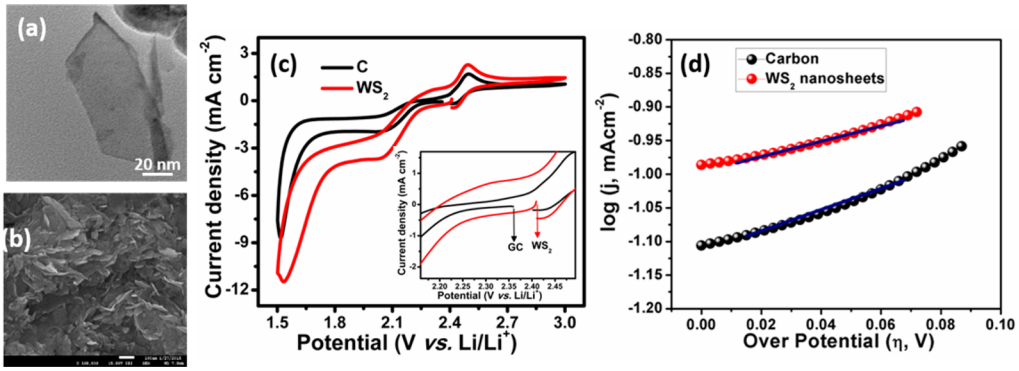

Figure 3. Morphology and electrocatalytic properties of shear-exfoliated WS_2 nanosheets. (a) TEM image of exfoliated WS_2. (b) SEM image of electrode composed of WS_2 nanosheets. (c) Comparative cyclic voltammograms of WS_2 nanosheets and carbon as a working electrode vs Li/Li^+ in catholyte solution. (Inset: Open-circuit potential with respect to electrode systems.) (d) Tafel plots for carbon and WS_2 nanosheet electrodes in catholyte electrolyte.

Table 1. Cumulative Electrocatalytic Properties of WS_2 Nanosheets and Carbon Electrodes toward Polysulfide Conversion Reactions

		onset potential (V)		peak current (mA)		exchange current density
electrode	OCV (V)	reduction (E_{pc})	oxidation (E_{pa})	reduction (I_{pc})	oxidation (I_{pa})	($\times 10^{-3}$ mA cm^{-2})
carbon	2.36	2.21, 1.67	2.42	8.5	1.71	8.5
WS_2	2.41	2.24, 1.78	2.39	11.5	2.35	11.8

DOI: 10.1021/jacs.6b08681
J. Am. Chem. Soc. 2017, 139, 171–178

Further, the kinetic behavior of WS_2 nanosheets can be understood by conducting LSV experiments (Supporting Information, Figure S7) on both electrodes at a scan rate of 0.1 mV s^{-1}. The exchange current density values were obtained from a Tafel plot, and the higher value for the WS_2 electrode (11.8 μA cm^{-2} against 8.5 μA cm^{-2}) confirms the facile kinetics for LiPS redox reactions (Figure 3d). Hence, superior electrocatalytic activity and reversibility of LiPS reactions using WS_2 nanosheets due to their exposed catalytic edge sites were favorable for better electrochemical performance.

3.3. Electrochemical Behavior. The electrochemical performance of WS_2 nanosheets and their bulk counterpart were evaluated by fabricating standard 2032 coin cells. The cells were assembled using WS_2 nanosheets and their bulk counterparts as working electrodes vs metallic lithium foil as counter/reference electrode and celgard membrane as a separator. Herein, the electrochemically active species (catholyte) was in the form of LiPS (600 mM of Li_2S_8) in TEGDME solution containing 1 M LiTFSI and 0.5 M $LiNO_3$. Electrochemical properties were measured at constant current rates of 0.2 and 0.5 C, with respect to a full discharge−charge capacity of 1672 mAh g^{-1} corresponds to 1C, in the potential window between 3.0 and 1.5 V.

Recorded CV curves for exfoliated electrode consist of two cathodic peaks at 2.44 and 1.9 V, corresponding to transformation of long-chain LiPSs to short-chain LiPS and subsequent reduction to end products, respectively (Figure 4a). Upon anodic

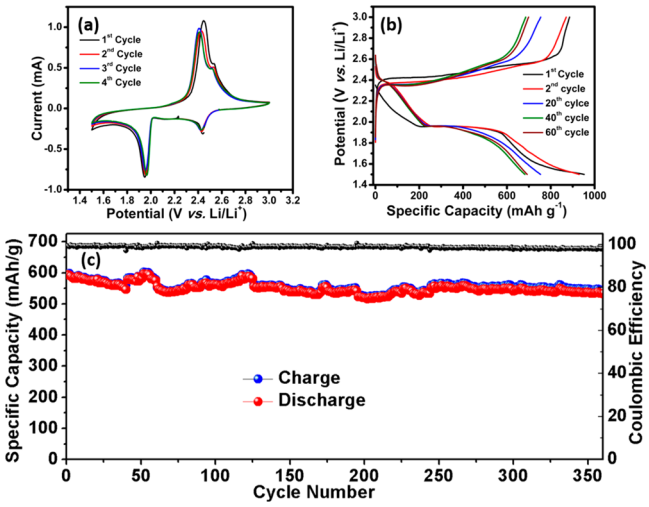

Figure 4. Electrochemical behavior. (a) Cyclic voltammograms of shear-exfoliated WS_2 nanosheets at a scan rate of 0.1 mV s^{-1}. (b) Charge−discharge profiles at 0.2 C rate and (c) cycling study of electrocatalytically active WS_2 nanosheets as working electrode vs Li/Li^+ with catholyte consisting of 600 mM Li_2S_8 at 0.5 C rate.

scan, a large anodic peak was observed at 2.42 V, which is related to reversible conversion of short-chain to long-chain LiPS,[48] along with a small peak at 2.53 V, attributed to formation of elemental sulfur; this reveals the excellent catalytic activity and stability of WS_2 nanosheets. Figure 4b reveals that an exfoliated electrode exhibited appreciable performance, with discharge plateaus around 2.4 and 2.0 V, with reduced polarization compared to its bulk counterpart (Supporting Information, Figure S8). Similarly, it has been observed to have a consistent capacity of 652 mAh g^{-1} at 0.2 C rate over 100 cycles (Supporting Information, Figure S9). Figure 4c evidences the cycling stability and Coulombic efficiency at 0.5 C rate, where a stable specific capacity of 596 mAh g^{-1} has been realized for 360 charge−discharge cycles. Most notably, excellent retention capacity (91%) and Coulombic efficiency are accomplished (99%) over the number of cycles due to effective polysulfide conversions on the newly identified electrocatalytically active WS_2 surface. On the other hand, the cycling behavior of the bulk WS_2 cathode demonstrates a stable capacity of 418 mAh g^{-1}, with a poor Coulombic efficiency of ∼98.5% due to limited catalytically active sites (Supporting Information, Figure S8b).

Herein, chemical stagnation against lithium intercalation of the WS_2 nanosheets electrode at the studied potential is verified by performing electrochemical studies (Supporting Information, Figure S10) with blank electrolyte (without polysulfides), implying its pure catalytic nature. As a control experiment, WS_2-free electrode was fabricated and showed poor electrochemical performance with 600 mM catholyte solution (Supporting Information, Figure S11). Furthermore, the shear-exfoliated WS_2 nanosheets are examined for high rate capability, and the results obtained are depicted in the Supporting Information (Figure S12). The electrode consisting of WS_2 nanosheets exhibited a capacity as high as 380 mAh g^{-1} at 1 C rate for more than 260 cycles. In addition, the significant specific retention capacity and columbic efficiency even at high charge−discharge rates studied have been noticed. Similarly, the compatibility of WS_2 nanosheets and solid sulfur as a electrode has been verified by performing experiments with polysulfide-free blank electrolyte (Supporting Information, Figure S13). Hence, using the electrocatalytically active phase as electrode toward LiPS conversions and stable battery performance is validated.

3.4. Electrocatalyst and LiPS Interactions. Evaluating interactions between LiPS and electrocatalyst is vital in designing better materials for Li−S batteries. The majority of prior studies have concentrated on determining adsorption characteristics, such as hydrophilicity, polarity, bond energies, etc., of the host material.[49−51] It was concluded that the formation of weak polythionate complexes during the initial discharge process makes some metal oxides and functionalized carbons preferable for preventing polysulfide migration.[13] However, these polythionate complexes were later found to be irreversible, especially when reduced graphene oxide was used in the electrode formulations.[13] As the formation of such irreversible reactions significantly affects the cycle life of a battery, it is important to design hydrophilic host structures that are also catalytically active toward polysulfide conversion reactions (Figure 5a). Thus, surface adsorption and reversible catalytic properties of WS_2 electrodes at various electrochemical conditions were probed using a combination of UV−vis, XPS, and SEM studies.

The vibrational and rotational modes of LiPS molecules, even at very low concentrations, are highly sensitive to UV−visible absorption. It is important to note that the solvent for LiPS greatly influences the absorption range. To examine the adsorption ability of lithium polysulfides on WS_2 nanosheets, we have used medium-chain-length Li_2S_4 (1 mL of 10 mM) as representative LiPS and verified its behavior with the addition of WS_2 nanosheets using a UV−vis study. A strong absorption peak has been observed at 610 nm which can be attributed to the dissolved LiPS and anion radicals such as $S_3^{\bullet-}$ (Figure 5b) in the solution.[52] Upon addition and precipitation of WS_2 (250 μg), a reduction in absorption peak intensity is observed, which indicates a decrease in LiPS concentration in the solution due to its strong adsorption on WS_2 nanosheets. Upon increasing

DOI: 10.1021/jacs.6b08681
J. Am. Chem. Soc. 2017, 139, 171−178

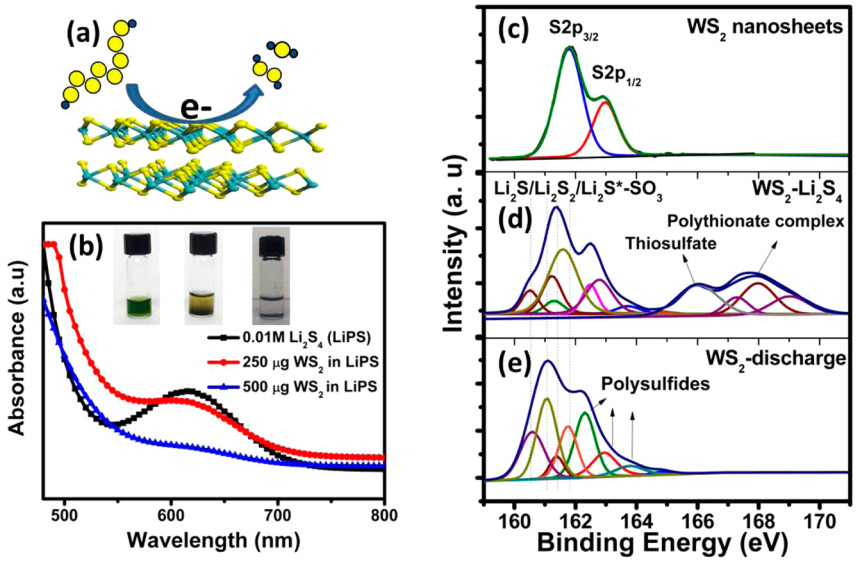

Figure 5. Electrocatalyst and LiPS interactions. (a) Pictorial representation of LiPS conversions on WS_2 nanosheets during discharge process. (b) UV−vis spectra of LiPS with variation in color upon adsorption on WS_2 nanosheets. (c−e) XPS study of core S 2p spectra of as-exfoliated WS_2 nanosheets (c), WS_2−Li_2S_4 (d), and WS_2 electrode at discharged state (e).

the WS_2 concentration (500 μg), the absorption peak intensity is completely diminished, confirming the strong affinity of LiPS toward sulfiphilic WS_2 nanosheets. On careful visual inspection, the same trends are recognized from the drastic color changes of the LiPS solution with the presence of WS_2 nanosheets, as shown in Figure 5b (inset).

The nature of the interactions between adsorbed species and WS_2 nanosheets (WS_2−Li_2S_4) is probed using XPS. To validate the same further during electrochemical cycling, the cycled cells containing WS_2 nanosheets electrodes were de-crimped cautiously at the end of the discharge, and XPS analysis was performed. Figure 5c−e presents the high-resolution XPS spectra of S_{2p} peaks corresponding to pristine WS_2 nanosheets, WS_2−Li_2S_4, and WS_2 electrode at discharge state, respectively. The S 2p core-level spectrum of WS_2 nanosheets displays typical peaks at 161.8 and 162.9 eV, which are corroborated to spin orbital states of S $2p_{3/2}$ and S $2p_{1/2}$ (Figure 5c). However, the S 2p spectra of the solid precipitate from the WS_2−Li_2S_4 solution displayed four predominant peaks, attributed to short-chain polysulfides with SO_3^- groups, polysulfides, thiosulfate, and polythiosulfate complexes, respectively. The thiosulfate complexes formed at 167.1 and 168.0 eV may originate from strong salt−solvent interactions with Li_2S_4 on WS_2 nanosheets during physical agitation (Figure 5d). Also, the same features were observed as soon as the polysulfides were exposed to the working electrode in cell fabrication (Supporting Information, Figure S14). Surprisingly, the peaks related to sulfate complexes are diminished upon complete discharge, which reflects the effect on an increase in intensity of short-chain LiPS peaks with the slight shift to lower binding energy values (Figure 5e). Hence, polysulfide conversions on the surface of WS_2 nanosheets in the presence of an electric field most likely occur at catalytically active edge sites. On the contrary, thiosulfate complexes which are formed on conventional carbon-based electrodes remain stable even at complete discharge, contributing to the loss of active material.[13,16] Further, owing to unsaturated sulfur atoms at the edge plane driving the electrocatalytic activity of WS_2 nanosheets, the reverse reaction, conversion from short-chain to long-chain polysulfides, is facile. On electrode surface speculation, SEM images of WS_2 nanosheet electrodes at the charged state reveal the absence of insoluble short-chain (Li_2S/Li_2S_2) LiPS. From SEM studies on cycled electrodes (Supporting Information, Figure S11), it is seen that WS_2 nanosheets are effective in converting short-chain to long-chain LiPS during the charging process, along with providing a surface for effective polysulfides conversion during discharge. Hence, electrocatalytically active electrodes are capable of adsorbing polysulfide species in a favorable manner to form short-chain LiPS and further converting them back during the cycling process.

4. DISCUSSION

We established the electrocatalysis approach in conjunction with sulfiphilic electrodes for an efficient conversion of lithium polysulfides during electrochemical cycling. In this regard, 2D WS_2 nanosheets were identified for their inherent physico-chemical and electrocatalytic properties such as adsorption of LiPS on its surface due to polarity and catalytic efficiency originating from their edge planes. An effective avenue for LiPS conversion reactions via catalytically active sites has been demonstrated successfully using CVD-grown WS_2 and MoS_2 nanosheets. Detailed microscopy and elemental mapping studies reveal that confined deposition of LiPS with dendrite-like structure all over the edges of the flakes was mainly due to unsaturated S atoms, which carry electronegativity for effective adsorption of lithium complexes. The derived catalytic properties, such as onset potential and redox peak potential/current and exchange current density values, confirmed the advantages of electrocatalytically active electrodes. Most importantly, the high electrocatalytic activity (8.53 mA cm^{-2}) of exfoliated WS_2 makes them attractive for LiPS redox reactions compared to carbon electrodes (2.52 mA cm^{-2}), wherein the presence of catalytic edge sites enhances the charge-transfer kinetics. Further, the synergism of WS_2 nanosheets (adsorption due to polarity and catalytic activity due to unsaturated S atoms at edge sites) on battery performance has been understood from galvanostatic charge−discharge measurements for over 100 cycles. From the studies, electrochemical properties such as specific

DOI: 10.1021/jacs.6b08681
J. Am. Chem. Soc. 2017, 139, 171−178

capacity (700 mAh g^{-1} at 0.2 C) and catalytic activity-driven stable Coulombic efficiency (99.4%) of WS_2 electrodes clearly support the usage of electrocatalytically active 2D materials as electrodes. Such stable electrochemical performance was corroborated to reversible interactions between electrocatalyst and LiPS, as understood from the UV−vis absorption and XPS studies. The significant reduction of polysulfide absorption peak intensity in the UV absorption spectra and the presence of strong XPS peaks corresponding to Li_2S_n species for the WS_2−Li_2S_4 sample revealed the desirable adsorption features of LiPS. The XPS study on cycled electrodes substantiates the long-chain to short-chain LiPS conversion mechanism through thiosulfate complexes and shows that their recombination occurs at unsaturated sulfur edge sites of WS_2 nanosheets.

5. SUMMARY

In summary, we have successfully demonstrated that the polysulfide shuttle in Li−S batteries can be stabilized using electrocatalytic transition metal dichalcogenide atomic layers. A combination of spectroscopic and microscopic analysis revealed that the *physicochemical* transformations at the electrode/electrolyte interface of monolayered/few-layered TMDs were reversible catalytic processes. A comprehensive investigation into the preferential active sites of XS_2 (X = Mo, W) materials for polysulfides' reactions, the electrocatalytic activity of WS_2 nanosheets, and the interface between WS_2 and Li_2S_n species was highlighted. As a result, the WS_2 electrode exhibited stable electrochemical performance via catalytically active edge sites, for instance, a specific capacity of 590 mAh g^{-1} with excellent Coulombic efficiency (99%) over 350 discharge−charge cycles. The advantages of this catalytic approach to Li−S batteries include the following: (i) as there is no physical encapsulation of polysulfides, the rate capability of lithium ions is not hindered; (ii) by employing TMDs, which are economically viable, the low cost advantage of sulfur batteries is retained; (iii) having a library of materials in the TMD family and using evolving synthesis techniques, it is possible to synthesize tailored material configurations; (iv) large-scale synthesis of such structures is feasible, making this approach easily adaptable for practical applications. Thus, the demonstrated electrocatalytic alternative approach using XS_2 (X = W, Mo) nanosheets for traditionally non-catalytic Li−S battery reactions is the first of its kind; it is expected to lay a strong evidence-based framework for the totally unexplored area of lithium−polysulfide electrocatalysis and provide a great avenue for theoretical and computational studies to predict better materials.

■ ASSOCIATED CONTENT

Supporting Information

The Supporting Information is available free of charge on the ACS Publications website at DOI: 10.1021/jacs.6b08681.

Characterizations of CVD-grown and shear-exfoliated WS_2 nanosheets and additional supplementary figures (PDF)

■ AUTHOR INFORMATION

Corresponding Author

*leela.arava@wayne.edu

ORCID

Leela Mohana Reddy Arava: 0000-0001-6685-6061

Notes

The authors declare no competing financial interest.

■ ACKNOWLEDGMENTS

L.M.R.A. acknowledges support from Wayne State University startup funds. We thank Dr. Eswaraiah Varrla, Nanyang Technological University, and Dr. Hemtej Gullapalli, Rice University, for their useful discussions.

■ REFERENCES

(1) Bruce, P. G.; Freunberger, S. A.; Hardwick, L. J.; Tarascon, J. M. *Nat. Mater.* **2012**, *11*, 19.
(2) Ogasawara, T.; Débart, A.; Holzapfel, M.; Novák, P.; Bruce, P. G. *J. Am. Chem. Soc.* **2006**, *128*, 1390.
(3) Cabana, J.; Monconduit, L.; Larcher, D.; Palacin, M. R. *Adv. Mater.* **2010**, *22*, E170.
(4) Zhang, H.; Yu, X.; Braun, P. V. *Nat. Nanotechnol.* **2011**, *6*, 277.
(5) Xiao, A.; Yang, L.; Lucht, B. L.; Kang, S.-H.; Abraham, D. P. *J. Electrochem. Soc.* **2009**, *156*, A318.
(6) Ji, X. L.; Nazar, L. F. *J. Mater. Chem.* **2010**, *20*, 9821.
(7) Demir-Cakan, R.; Morcrette, M.; Gangulibabu; Gueguen, A.; Dedryvere, R.; Tarascon, J.-M. *Energy Environ. Sci.* **2012**, *6*, 176.
(8) Ji, X.; Lee, K. T.; Nazar, L. F. *Nat. Mater.* **2009**, *8*, 500.
(9) Rauh, R. D.; Abraham, K. M.; Pearson, G. F.; Surprenant, J. K.; Brummer, S. B. *J. Electrochem. Soc.* **1979**, *126*, 523.
(10) Yamin, H.; Gorenshtein, A.; Penciner, J.; Sternberg, Y.; Peled, E. *J. Electrochem. Soc.* **1988**, *135*, 1045.
(11) Evers, S.; Nazar, L. F. *Acc. Chem. Res.* **2013**, *46*, 1135.
(12) Zhang, Q.; Wang, Y.; Seh, Z. W.; Fu, Z.; Zhang, R.; Cui, Y. *Nano Lett.* **2015**, *15*, 3780.
(13) Liang, X.; Hart, C.; Pang, Q.; Garsuch, A.; Weiss, T.; Nazar, L. F. *Nat. Commun.* **2015**, *6*, 5682.
(14) Liang, X.; Garsuch, A.; Nazar, L. F. *Angew. Chem., Int. Ed.* **2015**, *54*, 3907.
(15) Babu, G.; Ababtain, K.; Ng, K. Y. S.; Arava, L. M. R. *Sci. Rep.* **2015**, *5*, 8763.
(16) Al Salem, H.; Babu, G.; Rao, C. V; Arava, L. M. R. *J. Am. Chem. Soc.* **2015**, *137*, 11542.
(17) Bruix, A.; Füchtbauer, H. G.; Tuxen, A. K.; Walton, A. S.; Andersen, M.; Porsgaard, S.; Besenbacher, F.; Hammer, B.; Lauritsen, J. V. *ACS Nano* **2015**, *9*, 9322.
(18) Bonaccorso, F.; Colombo, L.; Yu, G.; Stoller, M.; Tozzini, V.; Ferrari, A. C.; Ruoff, R. S.; Pellegrini, V. *Science* **2015**, *347*, 1246501.
(19) Gao, M.-R.; Xu, Y.-F.; Jiang, J.; Yu, S.-H. *Chem. Soc. Rev.* **2013**, *42*, 2986.
(20) Chen, J.; Wu, X.-J.; Yin, L.; Li, B.; Hong, X.; Fan, Z.; Chen, B.; Xue, C.; Zhang, H. *Angew. Chem.* **2015**, *127*, 1226.
(21) Voiry, D.; Yamaguchi, H.; Li, J.; Silva, R.; Alves, D. C. B.; Fujita, T.; Chen, M.; Asefa, T.; Shenoy, V. B.; Eda, G.; Chhowalla, M. *Nat. Mater.* **2013**, *12*, 850.
(22) Yu, X.; Prevot, M. S.; Guijarro, N.; Sivula, K. *Nat. Commun.* **2015**, *6*, 7596.
(23) Lu, Q.; Yu, Y.; Ma, Q.; Chen, B.; Zhang, H. *Adv. Mater.* **2016**, *28*, 1917.
(24) Curtis, C. W.; Chen, J. H.; Tang, Y. *Energy Fuels* **1995**, *9*, 195.
(25) Fréty, R.; Breysse, M.; Lacroix, M.; Vrinat, M. *Bull. Soc. Chim. Belg.* **1984**, *93*, 663.
(26) Stephens, I. E. L.; Ducati, C.; Fray, D. J. *J. Electrochem. Soc.* **2013**, *160*, A757.
(27) Chhowalla, M.; Shin, H. S.; Eda, G.; Li, L.-J.; Loh, K. P.; Zhang, H. *Nat. Chem.* **2013**, *5*, 263.
(28) Gong, Y.; Lin, J.; Wang, X.; Shi, G.; Lei, S.; Lin, Z.; Zou, X.; Ye, G.; Vajtai, R.; Yakobson, B. I.; Terrones, H.; Terrones, M.; Tay, B. K.; Lou, J.; Pantelides, S. T.; Liu, Z.; Zhou, W.; Ajayan, P. M. *Nat. Mater.* **2014**, *13*, 1135.
(29) Pu, Z.; Liu, Q.; Asiri, A. M.; Obaid, A. Y.; Sun, X. *Electrochim. Acta* **2014**, *134*, 8.

DOI: 10.1021/jacs.6b08681
J. Am. Chem. Soc. 2017, 139, 171−178

(30) Chen, Z.; Cummins, D.; Reinecke, B. N.; Clark, E.; Sunkara, M. K.; Jaramillo, T. F. *Nano Lett.* **2011**, *11*, 4168.
(31) Shifa, T. A.; Wang, F.; Cheng, Z.; Zhan, X.; Wang, Z.; Liu, K.; Safdar, M.; Sun, L.; He, J. *Nanoscale* **2015**, *7*, 14760.
(32) Geng, X.; Sun, W.; Wu, W.; Chen, B.; Al-Hilo, A.; Benamara, M.; Zhu, H.; Watanabe, F.; Cui, J.; Chen, T.-p. *Nat. Commun.* **2016**, *7*, 10672.
(33) Cong, C.; Shang, J.; Wu, X.; Cao, B.; Peimyoo, N.; Qiu, C.; Sun, L.; Yu, T. *Adv. Opt. Mater.* **2014**, *2*, 131.
(34) van der Zande, A. M.; Huang, P. Y.; Chenet, D. A.; Berkelbach, T. C.; You, Y.; Lee, G.-H.; Heinz, T. F.; Reichman, D. R.; Muller, D. A.; Hone, J. C. *Nat. Mater.* **2013**, *12*, 554.
(35) Elias, A. L.; Perea-López, N.; Castro-Beltrán, A.; Berkdemir, A.; Lv, R.; Feng, S.; Long, A. D.; Hayashi, T.; Kim, Y. A.; Endo, M.; et al. *ACS Nano* **2013**, *7*, 5235.
(36) Kim, M. S.; Yun, S. J.; Lee, Y.; Seo, C.; Han, G. H.; Kim, K. K.; Lee, Y. H.; Kim, J. *ACS Nano* **2016**, *10*, 2399.
(37) Berkdemir, A.; Gutiérrez, H. R.; Botello-Méndez, A. R.; Perea-López, N.; Elías, A. L.; Chia, C.-I.; Wang, B.; Crespi, V. H.; López-Urías, F.; Charlier, J.-C.; Terrones, H.; Terrones, M. *Sci. Rep.* **2013**, *3*, 1755.
(38) Withers, F.; Bointon, T. H.; Hudson, D. C.; Craciun, M. F.; Russo, S. *Sci. Rep.* **2014**, *4*, 4967.
(39) Mao, D.; Wang, Y.; Ma, C.; Han, L.; Jiang, B.; Gan, X.; Hua, S.; Zhang, W.; Mei, T.; Zhao, J. *Sci. Rep.* **2015**, *5*, 7965.
(40) Wu, Z.; Fang, B.; Wang, Z.; Wang, C.; Liu, Z.; Liu, F.; Wang, W.; Alfantazi, A.; Wang, D.; Wilkinson, D. P. *ACS Catal.* **2013**, *3*, 2101.
(41) Lukowski, M. A.; Daniel, A. S.; English, C. R.; Meng, F.; Forticaux, A.; Hamers, R. J.; Jin, S. *Energy Environ. Sci.* **2014**, *7*, 2608.
(42) Wang, H.; Zhang, Q.; Yao, H.; Liang, Z.; Lee, H.-W.; Hsu, P.-C.; Zheng, G.; Cui, Y. *Nano Lett.* **2014**, *14*, 7138.
(43) Tour, J. M. *Nat. Mater.* **2014**, *13*, 545.
(44) Paton, K. R.; Varrla, E.; Backes, C.; Smith, R. J.; Khan, U.; O'Neill, A.; Boland, C.; Lotya, M.; Istrate, O. M.; King, P.; et al. *Nat. Mater.* **2014**, *13*, 624.
(45) Paton, K. R.; Varrla, E.; Backes, C.; Smith, R. J.; Khan, U.; O'Neill, A.; Boland, C.; Lotya, M.; Istrate, O. M.; King, P.; Higgins, T.; Barwich, S.; May, P.; Puczkarski, P.; Ahmed, I.; Moebius, M.; Pettersson, H.; Long, E.; Coelho, J.; O'Brien, S. E.; McGuire, E. K.; Sanchez, B. M.; Duesberg, G. S.; McEvoy, N.; Pennycook, T. J.; Downing, C.; Crossley, A.; Nicolosi, V.; Coleman, J. N. *Nat. Mater.* **2014**, *13*, 624.
(46) Varrla, E.; Backes, C.; Paton, K. R.; Harvey, A.; Gholamvand, Z.; McCauley, J.; Coleman, J. N. *Chem. Mater.* **2015**, *27*, 1129.
(47) Varrla, E.; Paton, K. R.; Backes, C.; Harvey, A.; Smith, R. J.; McCauley, J.; Coleman, J. N. *Nanoscale* **2014**, *6*, 11810.
(48) Fan, F. Y.; Woodford, W. H.; Li, Z.; Baram, N.; Smith, K. C.; Helal, A.; McKinley, G. H.; Carter, W. C.; Chiang, Y. M. *Nano Lett.* **2014**, *14*, 2210.
(49) Seh, Z. W.; Li, W.; Cha, J. J.; Zheng, G.; Yang, Y.; McDowell, M. T.; Hsu, P.-C.; Cui, Y. *Nat. Commun.* **2013**, *4*, 1331.
(50) Ji, X.; Evers, S.; Black, R.; Nazar, L. F. *Nat. Commun.* **2011**, *2*, 325.
(51) Lee, K. T.; Black, R.; Yim, T.; Ji, X.; Nazar, L. F. *Adv. Energy Mater.* **2012**, *2*, 1490.
(52) Ahn, S.; Yamakawa, S.; Akagi, K. *J. Mater. Chem. C* **2015**, *3*, 3960.

DOI: 10.1021/jacs.6b08681
J. Am. Chem. Soc. 2017, 139, 171−178